Original Article

MOLECULAR METABOLISM

LOX-1 rewires glutamine ammonia metabolism to drive liver fibrosis

Ruihua Huang[1], Hanyu Cui[1], Mohammed Abdulaziz Yahya Ali Alshami[1], Chuankui Fu[1], Wei Jiang[1], Mingyuan Cai[1], Shuhan Zhou[1], Xiaoyun Zhu[1,3,*], Changping Hu[1,2,4,]**

ABSTRACT

Objective: Liver fibrosis is a crucial condition for evaluating the prognosis of chronic liver disease. Lectin-1ike oxidized low density lipoprotein receptor-1 (LOX-1) has been shown potential research value and therapeutic targeting possibilities in different fibrotic diseases. However, the role of LOX-1 and the underlying mechanisms in liver fibrosis progression remain unclear.

Methods: LOX-1 expression was detected in liver tissues from patients and rodents with liver fibrosis. LOX-1 knockout rats were subjected to CCl_4 or methionine and choline-deficient diet (MCD) to induce liver fibrosis. Transcriptomic and metabolomics analysis were used to investigate the involvement and mechanism of LOX-1 on liver fibrosis.

Results: We found that LOX-1 exacerbated liver fibrosis by promoting hepatic stellate cells (HSCs) activation. LOX-1 deletion reversed the development of liver fibrosis. We further verified that LOX-1 drove liver fibrosis by reprogramming glutamine metabolism through mediating isoform switching of glutaminase (GLS). Mechanistically, we revealed the crucial role of the LOX-1/OCT1/GLS1 axis in the pathogenesis of liver fibrosis. Moreover, LOX-1 rewired ammonia metabolism by regulating glutamine metabolism—urea cycle to drive the progression of liver fibrosis.

Conclusions: Our findings uncover the pivotal role of LOX-1 in the progression of liver fibrosis, enrich the pathological significance of LOX-1 regulation of hepatic ammonia metabolism, and provide an insight into promising targets for the therapeutic strategy of liver fibrosis, demonstrating the potential clinical value of targeting LOX-1 in antifibrotic therapy.

Keywords LOX-1; GLS; Urea cycle; Liver fibrosis

1. INTRODUCTION

In responce to various harmful stimuli, such as hepatotoxins, hepatitis viruses, cholestasis, and nutritional or metabolic deficiencies, the liver initiates a coordinated reparative response aimed at limiting damage and restoring homeostasis [1,2]. This repair process typically begins with a transient but pronounced infiltration of immune cells and subsequent inflammation, which is followed by the activation and migration of myofibroblasts, resulting in increased synthesis and deposition of extracellular matrix (ECM) proteins [3—5]. Liver fibrosis, characterized by excessive ECM, is a reversible wound-healing response involving a range of cell types and mediators to encapsulate injury [6,7]. However, advanced fibrosis significantly contributes to liver -related morbidity and mortality and is strongly associated with progression to hepatocellular carcinoma (HCC) [8]. Although recent therapeutic agents (e.g., Resmetirom) have shown promising clinical efficacy in treating metabolic-dysfunction-associated steatohepatitis (MASH)-associated fibrosis fibrosis [9], liver fibrosis arising from diverse etiologies remain underdeveloped. Hepatic stellate cells (HSCs) are the primary source of ECM-producing fibroblasts in models of toxic, cholestatic, and metabolic liver diseases, including metabolic-dysfunction-associated steatosis liver disease (MASLD) [1,3]. HSCs are located in the subendothelial space of Disse, interposed between liver sinusoidal endothelial cells (LSECs) and hepatocytes [10]. Activation of HSCs into proliferating fibrillar myofibroblasts has been demonstrated as a central driver of liver fibrosis in both experimental and human liver injury [11]. During the regression of liver fibrosis, the reduction of hepatic myofibroblasts can occur through apoptosis or inactivation of activated HSCs [1]. Targeting the deactivation of HSCs into a quiescent-like state presents a promising therapeutic approach for fibrosis resolution [12].

In MASLD, disrupted hepatic cholesterol homeostasis leads to elevated levels of hepatic cholesterol, exacerbating the progression of liver injury [13]. Excessive free cholesterol also activates HSCs, indicating that cholesterol plays a significant role in MASLD-associated fibrogenesis [14,15]. Free cholesterol accumulation in HSCs is regulated by the low-density lipoprotein receptor (LDLR) through feedback regulation of cholesterol homeostasis [14,16]. Additionally, lectin-like oxidized LDL receptor 1 (LOX-1), a scavenger receptor responsible for the uptake of oxidatively modified LDL (oxLDL), promotes

[1]Xiangya School of Pharmaceutical Sciences, Central South University, Changsha 410013, China [2]School of Pharmacy, Changzhi Medical College, Changzhi 046000, Shanxi, China [3]Key Laboratory of Molecular Pharmacology and Drug Evaluation (Yantai University), Ministry of Education, Yantai University, Yantai, China [4]Hunan Provincial Key Laboratory of Cardiovascular Research, Changsha 410013 China

*Corresponding author. Xiangya School of Pharmaceutical Sciences, Central South University, Changsha 410013, China. E-mail: zhuxiaoyun@csu.edu.cn (X. Zhu).

**Corresponding author. Xiangya School of Pharmaceutical Sciences, Central South University, Changsha 410013, China. E-mail: huchangping@csu.edu.cn (C. Hu).

Received January 23, 2025 • Revision received March 21, 2025 • Accepted March 26, 2025 • Available online 1 April 2025

https://doi.org/10.1016/j.molmet.2025.102132

cholesterol accumulation and foam cell formation, exceeding the function of LDLR [17,18]. Recent studies have demonstrated that LOX-1 plays a critical role in lipid metabolism, oxidative stress and inflammatory responses during chronic liver disease, primarily through its interaction with oxLDL, thereby exacerbating hepatic steatosis and fibrogenesis [19–22]. Although LOX-1 has emerged as a promising therapeutic target not only for atherosclerotic cardiovascular disease but also for various fibrotic disorders [23–25], direct evidence elucidating its precise role and mechanisms in liver fibrosis remains limited. Thus, further investigations are required to clarify the mechanistic involvement of LOX-1 in hepatic fibrosis progression.

In this study, we investigated the mechanism and translational potential of LOX-1 in HSCs activation and liver fibrosis. Our data demonstrated that LOX-1 operated as an essential driver for HSCs activation and unveiled a potential novel target for the development of broad-spectrum anti-fibrotic therapies.

2. MATERIALS AND METHODS

2.1. Human liver samples

Collection and use of human tissue were ethically approved by Xiangya Hospital of Central South University (approval number: 202203718). Liver biopsies were collected from patients with liver fibrosis. Written informed consent was obtained from each patient. Normal people liver samples were purchased from Bioaitech (Xi'an, China). Information about the clinical liver samples was listed in Supplemental Table 1.

2.2. Tissue microarrays

Deidentified clinical tissue microarrays (TMAs) were purchased from Bioaitech (Xi'an, China). Tissue array patients information was shown in Supplementary Table 1.

2.3. Animal studies

Male Sprague–Dawley rats (6–8 weeks) and C57B6/J mice (6–8 weeks) were housed in an air-conditioned room at 25 °C with 12-h dark/light cycles. Wild type (WT) and LOX-1 knockout (*Lox-1*$^{-/-}$) rats were generated by Cyagen Biosciences (Suzhou, China), as previously described [26]. Rats received humane care with unlimited access to a chow diet and water during the whole study. Animal studies were approved by Institutional and Local Committee on the Care and Use of Animals of Central South University (approval number: CSU-2023-0115). All animals received humane care according to the National Institutes of Health (USA) guidelines. We complied with the principles of the 3Rs and respected the highest ethical and animal welfare standards in carrying out the animal experiments.

2.3.1. Rat models of liver fibrosis

To induce toxic liver fibrosis, rats were injected intraperitoneally (i.p.) with olive oil (n = 5) or 1 ml/kg carbon tetrachloride (CCl_4, 50% solution in olive oil, n = 8), twice a week for 6 weeks. Liver tissues were harvested at 48 h after the last injection of olive oil or CCl_4. To induce dietary liver fibrosis, rats were fed methionine choline-supplement diet (MCS, n = 5) or high-fat (45%), methionine (0.1%) choline-deficient diet (MCD) supplementing with 1% cholesterol (n = 8) up to 16 weeks. Liver tissues were fixed in paraformaldehyde for histology, or flash-frozen in liquid nitrogen and stored at −80 °C.

2.3.2. Mouse models of liver fibrosis

To induce toxic liver fibrosis, mice were injected intraperitoneally (i.p.) with olive oil or 2.5 ml/kg CCl_4 (10% solution in olive oil, n = 6), three times a week for 4 weeks. Liver tissues were harvested at 48 h after the last injection of olive oil or CCl_4. To induce cholestatic liver fibrosis, mice anesthetized with isoflurane through inhalation were subjected to bile duct ligation (BDL). The common bile duct was ligated twice with 6.0 silk sutures and cut through between the ligations. Sham-operated mice were subjected to laparotomy without BDL. The mice which received BDL or sham operation were sacrificed 14 days later (n = 6). Liver tissues were fixed in paraformaldehyde for histology, or flash-frozen in liquid nitrogen and stored at −80 °C.

2.4. Liver histological and immunohistological staining

Liver specimens were preserved in 4% paraformaldehyde and then dehydrated in a graded alcohol series. One part of liver tissues was embedded in paraffin blocks and cut into 4 μm sections. To examine hepatic morphology and assess liver fibrosis, hematoxylineeosin (H&E), Sirius red, and Masson's trichrome staining were performed. Tissue sections also were immunostained for LOX-1, α-SMA, F4/80, GLS1 and GLS2.

Ammonia staining was conducted as described previously [27]. Briefly, 4 μm paraffin embedded sections were dewaxed in xylene and hydrated through graded alcohols. Sections were washed in distilled water and incubated for 5 min with Nessler's reagent previously filtered with a 0.45 μm membrane. The sections were then washed briefly twice in distilled water, counterstained with haematoxylin, washed with running tap water, dehydrated in graded alcohol and mounted with DPX permanent mounting medium.

For Oil Red O staining, frozen liver sections were fixed in cold propylene glycol for 2 min and then incubated on slides in Oil Red O solution for 8 min. Sections were differentiated in 85% propylene glycol for 1 min, rinsed on slides with 2 changes of distilled water, incubated in hematoxylin for 2 min and softly rinsed on slides in tap water and 2 changes of distilled water. Sections were then coverslipped using an aqueous mounting medium. Images were visualized and scanned.

2.5. Immunohistofluorescence

Immunofluorenscent staining was performed according to the previous research [28]. For paraffin sections, deparaffination and rehydration were performed. Then, paraffin sections and cell culture slides were incubated by 5% BSA and incubated with mouse α-SMA and rabbit LOX-1 antibodies overnight at 4 °C. After washing, the slides were incubated for 2 h with Alexa Fluor 647 Donkey anti-Mouse IgG, Alexa Fluor 488 Donkey anti-Rabbit IgG. DAPI (Thermofisher, P36966) was used for nuclei staining. Immunofluorescent staining images were obtained by Zeiss LSM800.

2.6. Quantitative RT-PCR

Total RNA was extracted from the liver tissues of the rats or LX-2 cells using Tripure reagent (Roche Diagnostics, Indianapolis, IN) as described by the manufacturer. cDNA synthesis was carried out with HiScript® II Q Select RT SuperMix for qPCR (Vazyme). Quantitative PCR was performed in biological triplicates using SYBR Green reagent (Vazyme). The level of GAPDH RNA expression was used to normalize the data. PCR primer sequences are listed in Supplementary Table 2. A melting curve of each amplicon was determined to verify its specificity.

2.7. Western blotting

Proteins were extracted from the liver tissues or HSCs in the lysis buffer consisting of protease inhibitor cocktail. The extracted proteins were separated bypolyacrylamide SDS gel and electrophoretically transferred onto polyvinylidene fluoride membranes. The membranes were probed with the indicated antibodies over night at 4 °C.

Membranes were then incubated with a horseradish peroxidase coupled secondary antibody. Detection was performed using a ChemiDoc XRS+ (Bio-Rad). The relative expressions were quantified densitometrically using the Image Lab Works 4.0 software, and calculated according to the reference bands of ani-β-actin. Antibodies used in this study are listed in Supplementary Table 3.

2.8. Liver hydroxyproline content assay

Hydroxyproline (Hyp) content in livers was determined according to the Hyp assay kit's instruction manual. Hyp kit (A030-2-1) was purchased from Nanjing Jiancheng Bioengineering Institute (Nanjing, China). The data was expressed as Hyp (μg) per liver weight (mg).

2.9. Biochemical analysis

Aspartate aminotransferase (AST), alanine aminotransferase (ALT), ammonia levels in plasma were enzymatically measured as recommended by manufacturer's instructions (Nanjing Jiancheng Bioengineering Institute, Nanjing, China). Urea content in liver was determined according to the manufacturer's instructions (Beijing Solarbio Science & Technology Co.,Ltd.).

2.10. Cell culture

LX-2 and HEK293T cells were purchased from the Cell Bank of Chinese Academy of Sciences. Cells were cultured in Dulbecco's modified Eagle's medium (DMEM), supplemented with 10% fetal bovine serum (FBS) and 1% penicillin-streptomycin antibiotics. LX-2 and HEK293T cells were transfected with siRNA or plasmids using Lipofectamine RNAiMax transfection reagent. Sequences of siRNA were listed in the Supplementary Table 2. LOX-1-FLAG plasmids were constructed for the overexpression of LOX-1.

2.11. Primary rat liver cells isolation and culture

Isolation of primary rat HSCs, hepatocytes, and Kupffer cells was conducted as described previously [29]. Briefly, livers were digested with retrograde stepwise perfusion with solutions containing pronase and collagenase (Gibco, 17104019). The obtained cells were centrifuged at $50\times g$ for 3 min, to eliminate the majority of hepatocytes. After hepatocytes were pelleted, the non-parenchymal cells (NPC)-enriched precipitates were further centrifuged at $1350\times g$ for 15 min. GBSS/B solution containing 10% Nycodenz were added to the non-parenchymal cells and centrifuged at $1500\times g$ for 15 min to separate primary HSCs. The above Nycodenz layer was aspirated, 50% Percoll was added and centrifuged at $1500\times g$ for 15 min to obtain primary Kupffer cells. Cells were cultured in DMEM containing 10% FBS.

2.12. Cell viability assay

Cell viability was evaluated by CCK-8 assay (MCE, HY-K0301). Briefly, LX-2 cells were transfected with control siRNA or LOX-1 siRNA and plated in 96-well plates. At 24, 48, and 72 h, the CCK-8 solution was incubated with cells at 37 °C for 4 h. The absorbance was measured at 450 nm.

2.13. Flow cytometry

LX-2 cells were transfected with control siRNA or LOX-1 siRNA for 48 h. Cells were harvested, and cell apoptosis was analyzed using Annexin V-FITC/PI apoptosis detection kit (Yeason, 40302 ES) according to the protocols.

2.14. RNA-seq and data analysis

Using Trizol reagent, total RNA was isolated from the liver tissues of WT and *Lox-1*$^{-/-}$ rats injected by CCl_4. The library was constructed and sequenced by Guangzhou Ribobio Co., LTD. The differential expression analysis was performed using the DESeq2. $|\log_2(\text{Fold Change})|$ of expressed genes >1 and P value <0.05 were considered to be significantly different expressed genes. The RNA-seq data files have been deposited to the Sequence Read Archive (SRA) database under accession number PRJNA1093279.

2.15. Metabolomics analysis

Metabolites were detected by MetWare (http://www.metware.cn/) based on the AB Sciex QTRAP 6500 LC-MS/MS platform.

2.16. Co-immunoprecipitation (Co-IP)

Co-immunoprecipitation (Co-IP) was performed as described previously [30]. LX-2 and HEK293T cells were transfected with empty vector or LOX-1-FLAG plasmids for 48 h. Cells were lysed in WB/IP lysis buffer (Yeasen, 20118ES60) containing protease inhibitor cocktail (MCE, HY-K0010). The supernatant of cell lysates was precleared by IP-grade antibodies against FLAG, LOX-1 or control IgG. After gentle rocking at 4 °C for 2 h, Protein A/G PLUS-Agarose (Santa Cruz Biotechnology, CA, USA) was added to the lysate/antibody mixture and incubated with gentle agitation at 4 °C overnight. Then the immunoprecipitates were collected by centrifugation and washed three times with PBS, then boiled for 5 min with the same volume of 2× loading buffer (Bio-Rad, 1610737). Proteins were resolved by 10% SDS-PAGE and subjected to Western blotting. Representative blots were presented.

2.17. Luciferase reporter assay

The full-length human *Gls1* promoter (−2000 to 0 relative to the transcription start site, 2001 base pairs total length) and four truncations of the *Gls1* promoter (divided into −2000 to −1501, −1500 to −1001, −1000 to −501, −500 to 0 relative to the transcription start site, 500 base pairs total length each truncation) were cloned by PCR amplification and incorporating restriction sites for KpnI and XhoI. The promoters were then subcloned into the luciferase reporter vector pGL4.17, generating the indicated luciferase reporter plasmids. The luciferase reporter plasmids containing the promoter of human *Gls1* gene were transfected into LX-2 and HEK293T cells. Cells were cultured for additional 48 h before harvest and the luciferase activity was measured using the Dual Luciferase Reporter Assay kit (Vazyme, DL101) based on the instructions of the kit.

2.18. CUT&RUN qPCR

CUT&RUN qPCR was performed according to the manufacturer's instructions (Vazyme, HD101). In brief, 5 million cells were permeabilized with 0.02% digitonin. Pellets were washed and incubated with antibody buffer containing OCT1 antibody at room temperature for 2 h with rotation. Followed by washing, the pellets were incubated with pA-MNase at 4 °C for 1 h. Targeting digestion was initiated by adding 100 mM $CaCl_2$ to a final concentration of 2 mM. The digestion was stopped by mixing in 2× STOP solution. Solubilized chromatin fragments were released and purified for qPCR.

2.19. NH_4Cl treatment

LX-2 cells were cultured with DMEM without serum and glutamine for 24 h. Then LX-2 cells were transfected with control siRNA or LOX-1 siRNA and simultaneously treated with NH_4Cl for 48 h.

2.20. Statistical analysis

All analyses were performed using GraphPad Prism 10 software. Statistical analyses were performed applying a two-tailed Student's t-

test or one-way ANOVA with Student-Newman-Keuls post hoc analysis, where indicated. Error bars in figures represent the standard deviation. Animals were randomized into groups. Samples were randomized for metabolomics analysis. The investigators were not blinded to allocation during experiments.

3. RESULTS

3.1. LOX-1 may be an essential driver of liver fibrosis in both humans and rodents

To evaluate the role of LOX-1 in the development of liver fibrosis, we initially characterized LOX-1 expression in normal and fibrotic liver specimens from the Gene Expression Omnibus (GEO) database. It was found that hepatic LOX-1 mRNA expression was upregulated in patients with MASH as well as rats with cirrhosis (Figure 1A). Similarly, elevated LOX-1 mRNA expression was observed in patients with alcoholic fatty liver (Fig. S1a). To further investigate the relevance of LOX-1 in human hepatic fibrosis, liver sections from human subjects were examined. Compared to controls, patients with fibrotic livers exhibited significantly higher LOX-1 protein expression (Fig. S1b, Figure 1B), which was positively correlated with liver fibrosis stage and α-SMA expression (Figure 1B). Meanwhile, we found that LOX-1 protein levels was positively correlated with human plasma AST and ALT levels (Figure 1C). Consistent with these findings, LOX-1 mRNA and protein expression was significantly increased in rat models of liver fibrosis induced by CCl_4 or methionine (1%) choline-deficient diet (MCD) (Figure 1D—F), as well as in mice induced by CCl_4 and BDL (Fig. S1c). To determine the cellular distribution of LOX-1, LOX-1 expression was examined in cultured primary HSCs, hepatocytes, and kupffer cells isolated from healthy rats. Results showed that LOX-1 was predominantly expressed in HSCs, even though the expression of LOX-1 was also observed in hepatocytes and kupffer cells (Figure 1G). Furthermore, liver immunofluorescence staining demonstrated co-localization of LOX-1 with α-SMA-positive HSCs (Figure 1B and Fig. S1d).

The above results collectively indicated that LOX-1 expression in the liver was increased during the progression of liver fibrosis in both humans and rodents. Considering LOX-1 was predominantly expressed in HSCs, our study focused on the function of LOX-1 in HSCs activation during liver fibrosis.

3.2. LOX-1 deficiency ameliorated chemical and diet-induced liver fibrosis in rats

To further investigate the causal relationship between LOX-1 and liver fibrosis, fibrogenesis was explored in *Lox-1* knockout (*Lox-1*$^{-/-}$) rats subjected to CCl_4 and MCD treatment. There was no significant difference in body weight gain between WT and LOX-1$^{-/-}$ rats subjected to CCl_4 and MCD treatment (Fig. S2a). WT and *Lox-1*$^{-/-}$ rats were injected with CCl_4 to induce liver fibrosis, and the ratio of liver weight/body weight were recorded which showed no significant difference between WT and *Lox-1*$^{-/-}$ rats (Figure 2A). Genetic deficiency of *Lox-1* effectively ameliorated CCl_4-induced hepatic injury and inflammatory cell infiltration, indicated by the plasma AST and ALT level and H&E staining (Figure 2B—C). Masson's trichrome and Sirius red staining, as well as hydroxyproline content determination exhibited that injection of CCl_4 leading to collagen deposition were attenuated by *Lox-1* deletion (Figure 2C—D). Complementally, the expression of α-SMA, a marker of activated HSCs and liver fibrosis, was decreased in conjunction with *Lox-1* knockout (Figure 2A). Concordant with the histological reversal of fibrosis, *Lox-1* countered the upregulation of fibrosis-related gene signatures caused by CCl_4, such as *Acta2*, *Col1a1*, *Timp1*, *Tgf-β1*, *Pdgf-A* (Figure 2F).

For another thing, WT rats fed a MCD diet for 16 weeks exhibited higher liver weight-to-body weight ratios, although this increase was not significantly reduced in *Lox-1*$^{-/-}$ rats (Figure 3A). Consistent with CCl_4 models, LOX-1 deficiency recovered plasma levels of AST and ALT induced by MCD diet (Figure 3B). H&E and oil red O staining revealed severe hepatic steatosis in WT rats under the MCD diet feeding condition, and less lipid droplets were seen in *Lox-1*$^{-/-}$ rats (Figure 3C). In addition, WT rats fed the MCD diet displayed severe fibrosis phenotypes, as revealed by larger Masson's and Sirius red staining positive areas, along with higher hydroxyproline levels, which was reversed in *Lox-1*$^{-/-}$ rats (Figure 3C—D). Hepatic fibrogenesis, as indicated by increased α-SMA levels and profibrotic gene expression in WT rats fed the MCD diet, was significantly attenuated in *Lox-1*$^{-/-}$ rats (Figure 3E—F).

Considering that hepatic fibrosis results from sustained chronic inflammation [4], we analyzed inflammatory markers in livers obtained from CCl_4 and MCD induced fibrotic rat models by performing IHC staining for the inflammatory marker F4/80 and assessing hepatic mRNA expression levels of pro-inflammatory cytokines TNFα, and IL-6. As anticipated, hepatic expression of *Tnfα*, *Il-6* and F4/80 was increased in both fibrotic models. Notably, LOX-1 genetic knockout attenuated these inflammatory responses in the liver (Figs. S2b—c). Overall, these findings revealed that genetic deletion of LOX-1 alleviated liver fibrosis.

3.3. LOX-1 was required for the fibrogenic activation in HSCs

As mentioned above, LOX-1 expression was predominantly observed in HSCs. Activated HSCs are the key source of excess extracellular matrix exacerbating liver fibrosis [12]. To investigate whether LOX-1 regulates HSCs activation during liver fibrosis, we examined the gradual increased expression of LOX-1 with the extending of incubation time in activated WT HSCs, which correlated positively with α-SMA expression (Figure 4A,B). As expected, we observed that LOX-1 expression was mostly colocalized with a-SMA-expressing myofibroblasts in activated HSCs (Figure 4B). We further evaluated the transdifferentiation of primary HSCs isolated from *Lox-1*$^{-/-}$ rats compared to those isolated from WT rats. HSCs from *Lox-1*$^{-/-}$ rats showed decreased expression of myofibroblast marker protein a-SMA, exhibiting a less efficient pattern of transdifferentiation into myofibroblasts compared with WT HSCs (Figure 4C,D). In addition, we used LOX-1 siRNA to knock down *Lox-1* expression in the immortalized human HSCs strain LX-2. Similarly, LOX-1 knockdown resulted in decreased α-SMA and COL1A1 protein expression (Figure 4E). Besides, we observed that the fluorescence intensity of α-SMA was diminished with LOX-1 knockdown (Figure 4F). Reduced expression of the profibrotic genes in *Lox-1*$^{-/-}$ LX-2 cells also suggested the effect of LOX-1 knockdown on suppressing HSCs activation (Figure 4G). To further confirm whether LOX-1 knockdown effectively reverse HSC activation, we transfected primary cultured HSCs derived from WT rats with LOX-1 siRNA. As anticipated, LOX-1 silencing inhibited primary HSC activation (Fig. S3a). Moreover, LOX-1 silencing inhibited TGF-β1 induced activation of LX-2 cells (Fig. S3b). To corroborate these findings, we utilized BI-0115, a selective LOX-1inhibitor, to treat LX-2 cells as well as primary cultured HSCs (Fig. S3c). Collectively, these experiments provided robust evidence that genetic silencing or pharmacological inhibition of LOX-1 effectively attenuated HSC activation, thereby reinforcing LOX-1 as a promising therapeutic target for liver fibrosis. Additionally, CCK-8 assays examined disrupted proliferation and flow

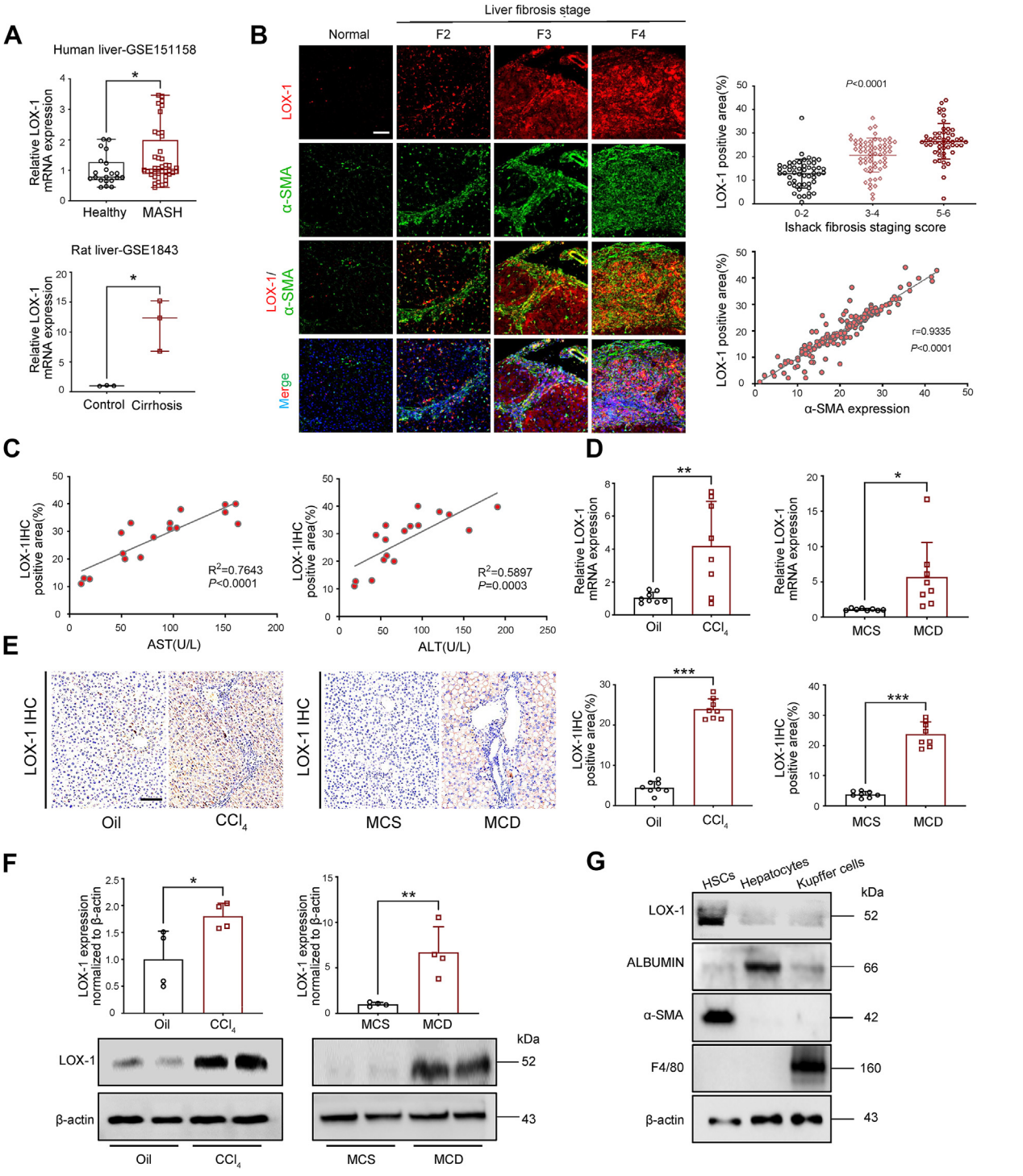

Figure 1: LOX-1 may be an essential driver of MASLD in both humans and rodents. A, Box plots of relative *Lox*-1 mRNA levels in GSE151158, GSE1843 datasets. **B**, Double immunofluorescence staining for LOX-1 (red) and α-SMA (green) in normal and fibrotic human livers (10 normal and 100 fibrotic liver tissue spots). Scale bars, 50 μm. Correlation analysis of LOX-1 expression with Ishak fibrosis staging scores. The positive correlation of LOX-1 with α-SMA in patients with fibrosis from tissue arrays. **C**, Correlation analysis of LOX-1 expression with AST levels (left) and ALT levels (right) of human specimen. **D**, Gene expression of *Lox-1* in WT rat liver tissues. **E**, Representative images of LOX-1 IHC in WT rat liver tissues (left). Scale bars, 50 μm. Quantitative analysis of LOX-1 IHC (right). **F**, Immunoblot and quantitative analysis of LOX-1 in WT rat liver tissues. **G**, Immunoblot of LOX-1, ALBUMIN (biomarker of hepatocytes), α-SMA (biomarker of HSCs), F4/80 (biomarker of Kupffer cells) on primary HSCs, hepatocytes and Kupffer cells from WT rats. Data are presented as mean ± s.d. *P* value were calculated using a two-tailed Student's *t*-test (**A**, **D, E** and **F**); $*P < 0.05$; $**P < 0.01$; $***P < 0.001$. (For interpretation of the references to color in this figure legend, the reader is referred to the Web version of this article).

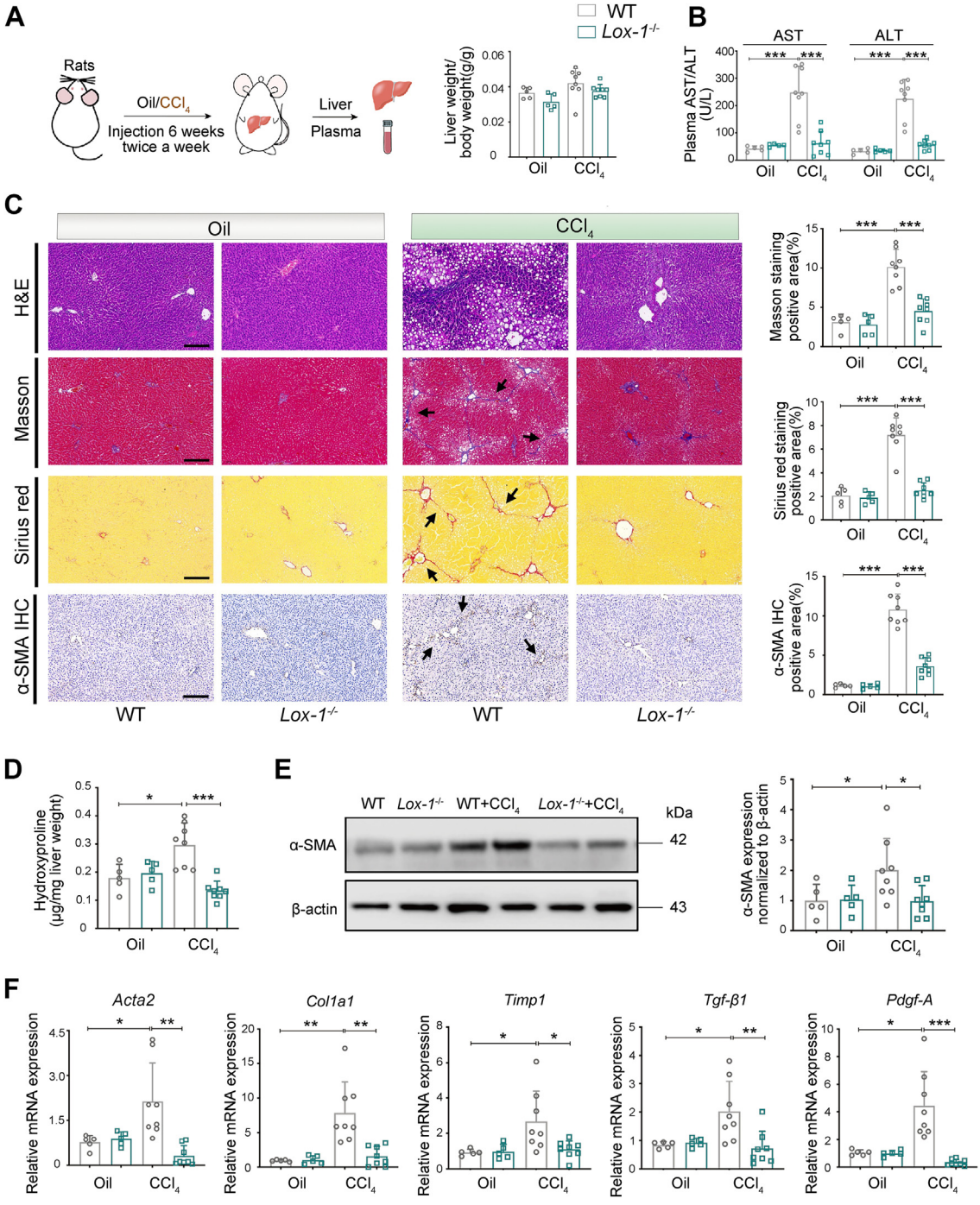

Figure 2: LOX-1 deficiency inhibited CCl_4-induced liver fibrosis in rats. A-I, Rats were injected intraperitoneally of olive oil or CCl_4 at the dose of 2 ml/kg twice a week for 6 weeks (n = 5 for each group of rats treated with olive oil; n = 8 for each group of rats treated with CCl_4). Liver and plasma were collected for subsequent experiments. **A**, Schematic of Oil/CCl_4-injected WT rats and *Lox-1*$^{-/-}$ rats (left). Liver/body weight of rats (right). **B**, Plasma AST and ALT levels. **C**, Representative images and quantification of H&E, Masson's trichrome, Sirius red staining and α-SMA IHC of liver sections. Arrows indicated the fibrotic areas. Scale bars, 100 μm. **D**, Liver hydroxylproline levels. **E**, Immunoblots and quantification for α-SMA in liver tissues. **F**, mRNA levels of genes related to liver fibrosis. Data are presented as mean ± s.d. *P* values were calculated using one-way ANOVA with Student-Newman-Keuls post hoc analysis (**A-F**); $^{*}P < 0.05$; $^{**}P < 0.01$; $^{***}P < 0.001$.

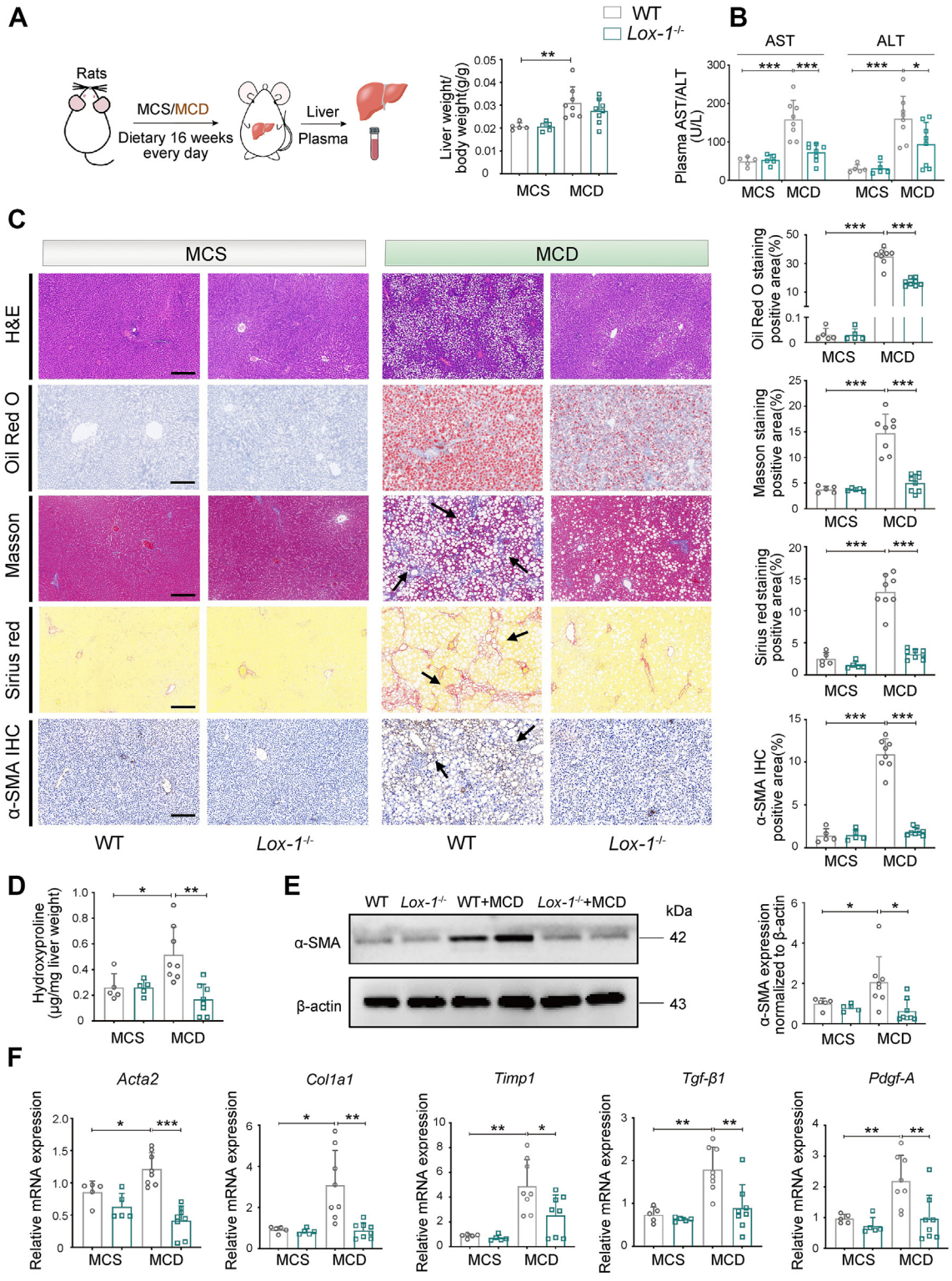

Figure 3: LOX-1 deficiency inhibited MCD-induced liver fibrosis in rats. A-J, Rats were fed with MCS/MCD diet every day for 16 weeks (n = 5 for each group of rats fed with MCS; n = 8 for each group of rats fed with MCD). Liver and plasma were collected for subsequent experiments. **A**, Schematic of MCS/MCD-fed WT rats and *Lox-1*$^{-/-}$ rats (left). Liver/body weight of rats (right). **B**, Plasma AST and Plasma ALT levels. **C**, Representative images and quantification of H&E, Oil Red O, Masson's trichrome, Sirius red staining and α-SMA IHC of liver sections. Arrows indicated the fibrotic areas. Scale bars, 100 μm. **D**, Liver hydroxylproline levels. **E**, Immunoblots and quantification for α-SMA in liver tissues. **F**, mRNA levels of genes related to liver fibrosis. Data are presented as mean ± s.d. *P* values were calculated using one-way ANOVA with Student-Newman-Keuls post hoc analysis (**A-F**); $^{*}P < 0.05$; $^{**}P < 0.01$; $^{***}P < 0.001$.

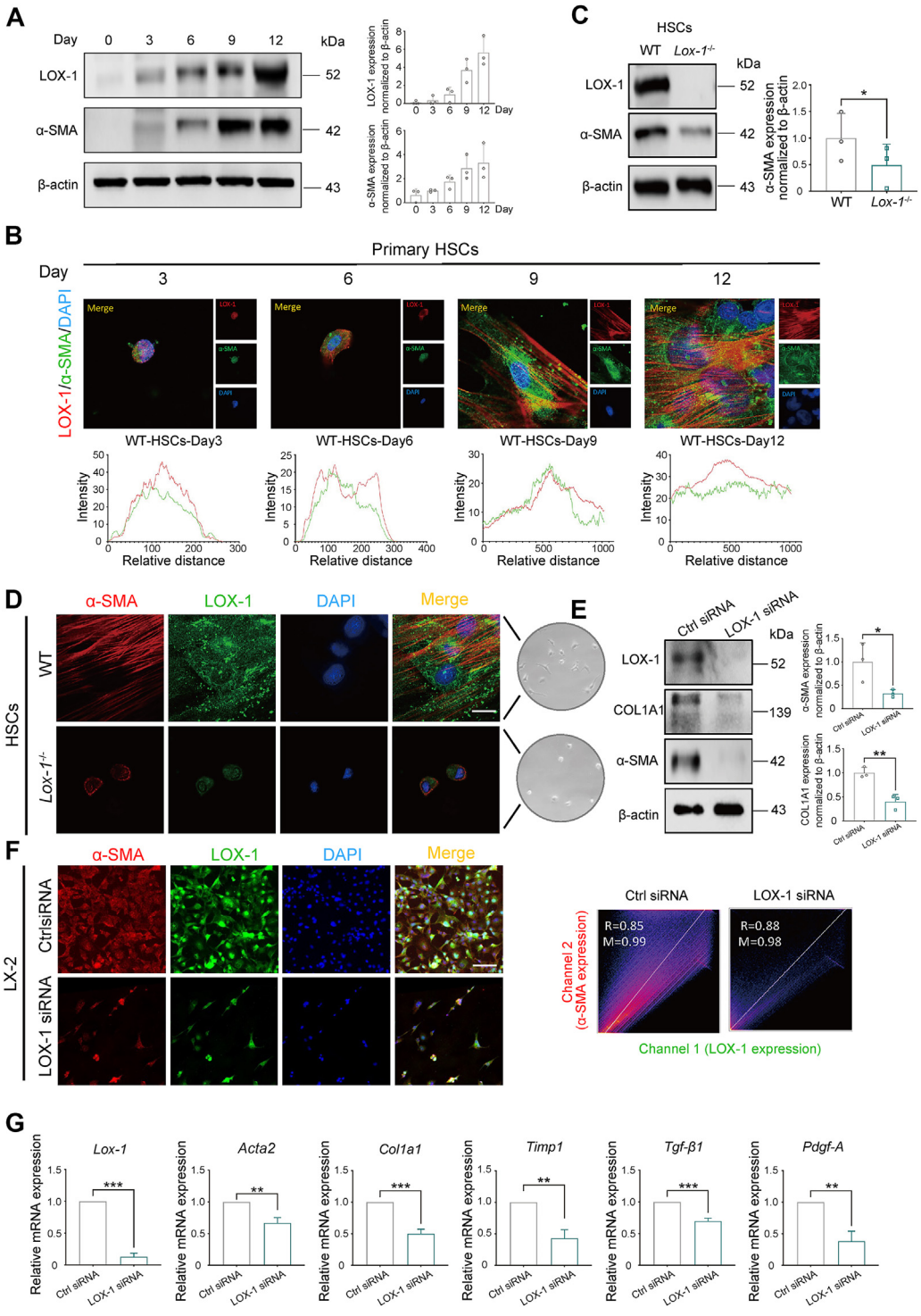

Figure 4: LOX-1 was required for the fibrogenic activation in HSCs. A, Immunoblots and quantification for LOX-1 and α-SMA in cultured primary HSCs from WT rats without treatment at the indicated times. **B**, Double immunofluorescence staining for LOX-1 (green) and α-SMA (red) in cultured primary HSCs from WT rats (top). Scale bars, 20 μm. Intensity of LOX-1 (green) and α-SMA (red) staining (below). **C**, Immunoblots and quantification for LOX-1 and α-SMA in cultured HSCs from WT and *Lox-1*$^{-/-}$ rats (9 days). **D**, Double immunofluorescence staining for LOX-1 and α-SMA in cultured HSCs from WT and *Lox-1*$^{-/-}$ rats (9 days). Scale bars, 20 μm. **E**, Immunoblotting assays of LOX-1, α-SMA and collagen I in LX-2 cells transfected with control or LOX-1 siRNA. **F**, Double immunofluorescence staining for LOX-1 (green) and α-SMA (red) in LX-2 cells transfected with control or LOX-1 siRNA (left). Scale bars, 50 μm. Fluorescence images on the left were subjected to colocalization analyses using the Coloc2 plugin in Image J (right). The pixel intensity correlation of channels 1 and 2 over space was depicted as a 2D scatterplot. Pearson correlation analysis and Mander's overlap coefficient were used to test the significance of correlation and were judged positively correlated when >0.5. **G**, Profibrotic genes expression was examined by qPCR in LX-2 cells transfected with control or LOX-1 siRNA. Data are presented as mean ± s.d. *P* values were calculated using a two-tailed Student's *t*-test (**c**, **e** and **g**); $^{*}P < 0.05$; $^{**}P < 0.01$; $^{***}P < 0.001$.

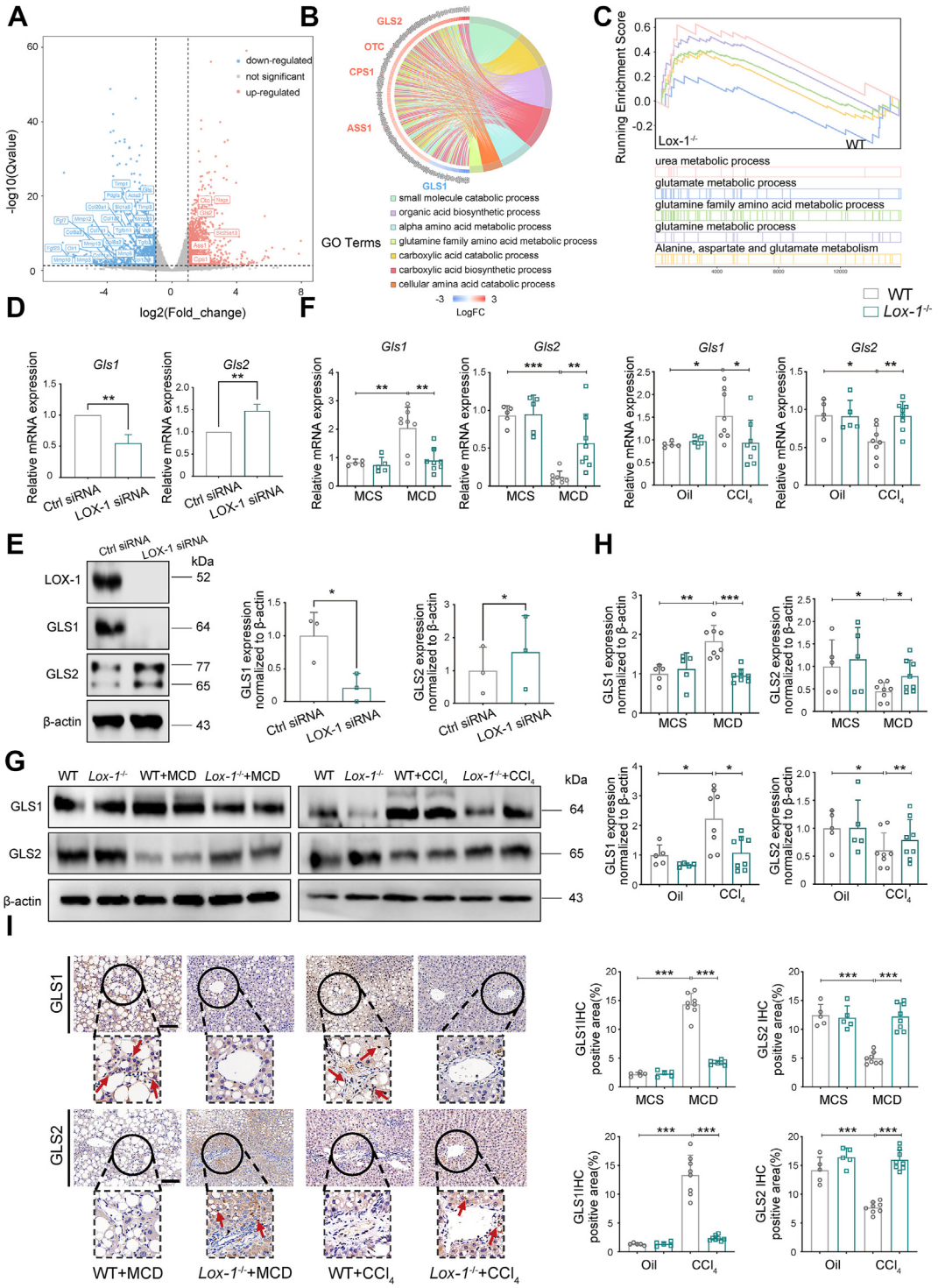

Figure 5: LOX-1 reprogrammed glutamine metabolism to promote liver fibrosis in rats. A-C, Liver tissues harvested from CCl_4-induced WT and *Lox-1*$^{-/-}$ rats. RNA-sequencing was performed as described in Methods. **A**, Volcano plot of DEGs. The up-regulated DEGs (red) and down-regulated DEGs (blue) were labeled. **B**, Chord diagram showing GO-enriched items of DEGs. **C**, Enrichment of pathways related to glutamine metabolism, as analyzed by GSEA of RNA-seq data. **D-E**, LX-2 cells were transfected with control or LOX-1 siRNA for 48 h. **D**, mRNA levels of *Gls1* and *Gls2*. **E**, Protein levels of GLS1 and GLS2. **F-I**, Liver tissues harvested from MCD and CCl_4-induced WT and *Lox-1*$^{-/-}$ rats. **F**, mRNA levels of *Gls1* and *Gls2*. **G-H**, Protein levels of GLS1 and GLS2. **I**, Representative images and quantification of GLS1 and GLS2 IHC. Scale bars, 20—50 μm. Data are presented as mean ± s.d. *P* values were calculated using a two-tailed Student's *t*-test (**D** and **E**) or one-way ANOVA with Student-Newman-Keuls post hoc analysis (**F**, **H**, **G** and **I**); $^{*}P < 0.05$; $^{**}P < 0.01$; $^{***}P < 0.001$.

cytometry analysis demonstrated a marginal increase in apoptosis in LX-2 cells upon LOX-1 depletion (Figs. S3d—e). Conversely, overexpression of LOX-1 using LOX-1-FLAG plasmids, as well as stimulaton of endogenous LOX-1 expression by oxLDL, exacerbated HSCs activation, as evidenced by increased expression of profibrogenic genes (Figs. S4a—c). Collectively, these findings suggested that LOX-1 may play an integral role in HSCs transdifferentiation.

3.4. LOX-1 rewired glutamine metabolism to drive liver fibrosis in rats

To investigate the transcriptional mechanism which LOX-1 may programme HSCs activation and liver fibrosis, we conducted RNA-sequencing analysis on liver samples obtained from WT and *Lox-1*$^{-/-}$ rats treated with CCl_4. The genetic ablation of LOX-1 had a profound impact on the rat liver transcriptome associated with liver fibrosis (Fig. S5a). Furthermore, Gene ontology (GO) analysis revealed that LOX-1 deficiency primarily affected genes related to pathways associated with amino acid metabolism, particularly the metabolic process of glutamine family amino acid (including glutamine, glutamate, alanine, aspartate, asparagine, histidine, ornithine and lysine) (Figure 5B). Additionally, we employed gene set enrichment analysis (GSEA) to identify the key genes involved in glutamine-ammonia related metabolism pathways and found that the genetic deletion of LOX-1 increased the occurrence of glutamine-ammonia metabolic routes in CCl_4-induced liver fibrosis (Figure 5C).

To elucidate the mechanism that LOX-1 influenced the shift in glutamine nitrogen metabolism to contribute to the progression of liver fibrosis, we focused on the genes involving in glutamine-ammonia metabolism. Among these genes, Glutaminase (GLS) 1 and GLS2 showed the most significant alteration (Fig. S5b). Consistent with previous researches [31,32], analysis of fibrotic human liver specimens indicated an elevated expression of GLS1 and decreased expression of GLS2 compared to healthy controls (Fig. S5c). GLS, an enzyme responsible for the initial step of glutamine metabolism by converting glutamine to glutamate and ammonia, consists of two forms: GLS1 and GLS2 [33]. GLS has been identified as a critical metabolic enzyme involved in chronic liver injury and fibrosis [34]. Consequently, we investigated the influence of LOX-1 on glutamine metabolism by assessing the expression of GLS1 and GLS2 in activated HSCs and fibrotic livers. The data revealed that the knockdown of LOX-1 in LX-2 cells resulted in decreased GLS1 expression and increased GLS2 expression (Figure 5D—E). Additionally, the overexpression of LOX-1 in LX-2 cells led to an increase in GLS1 levels and a decrease in GLS2 levels (Figs. S5d—e). Corresponding with the results in LX-2 cells, fibrotic liver induced by CCl_4 and MCD showed higher expression of GLS1 and lower expression of GLS2 compared to control groups, while LOX-1 ablation reversed these trends (Figure 5F—I, Fig. S5f). Further, we performed immunoblotting analyses to evaluate the expression of two GLS1 isoforms (GAC and KGA) in liver tissues from rats subjected to CCl_4 and MCD induced fibrosis. Consistent with previous reports, our results demonstrated significant upregulation of both GAC and KGA isoforms in fibrotic livers. Importantly, LOX-1 deficiency markedly attenuated the increased expression of these GLS1 isoforms in both fibrotic models (Fig. S5g).

In order to further elucidate the impact of glutamine catabolism on HSCs activation, we examined the mRNA expression of profibrogenic genes upon knocking down GLS1 or GLS2 (Figs. S6a—b). The deficiency of GLS1 diminished HSCs activation, while GLS2 expression was elevated. Importantly, the deficiency of GLS2 exacerbated HSCs activation without affecting GLS1 expression. To investigate the functional relevance of GLS1-mediated glutaminolysis in HSCs activation, we treated LX-2 cells with BPTES (Bis-2-(5-phenylacetamido-1,3,4-thiadiazol-2-yl) ethylsulfide), a specific inhibitor of GLS1. Simultaneously, we overexpressed LOX-1 and observed that GLS1 inhibition overcame the promoting effect of LOX-1 overexpression on HSCs activation (Fig. S6c).

Overall, these findings indicated that targeting LOX-1 may alleviate HSCs activation and liver fibrosis by reprogramming glutamine-ammonia metabolism.

3.5. LOX-1 promoted GLS1-mediated glutaminolysis via OCT1

The above results have indicated that LOX-1 reprogrammed glutamine metabolism to promote HSCs activation, and the use of GLS1 inhibitor BPTES reversed HSCs activation stimulated by LOX-1 overexpression. Accordingly, we further investigated the molecular mechanism of LOX-1 regulation of GLS1. As reported in previous researches [35,36], it has been corroborated that a positive feedback loop further upregulated octamer-binding transcription factor (OCT1, encoded by *Pou2f1*) expression in an oxLDL/LOX-1-dependent manner. Consistent with previous studies, we confirmed that stimulation of LOX-1 with oxLDL led to an increase in *Pou2f1* expression in LX-2 cells (Fig. S7a). Interestingly, we observed a downregulation of *Pou2f1* mRNA expression upon repression of LOX-1 in LX-2 cells, but not in 293T cells (Fig. S7b). We speculated that the interaction of LOX-1 with OCT1 could only be triggered on account of the self-activation mechanism of hepatic stellate cells. Furthermore, utilizing co-immunoprecipitation (Co-IP) experiments, we verified the interaction between LOX-1 and OCT1 in LX-2 and 293T cells, which was enhanced by LOX-1 overexpression (Figure 6A,B). Similarly, in fibrotic rat livers triggered by CCl_4 and MCD treatment, genetic ablation of LOX-1 resulted in a decrease in OCT1 protein expression (Fig. S7c). Utilizing JASPAR predictions, we identified several potential OCT1 binding sites in the promoter region of GLS1 (Figure 6C). To elucidate the regulatory mechanism of LOX-1 on GLS1 expression in the context of liver fibrosis, we investigated whether OCT1 functioned as a modulator of GLS1. CUT&RUN qPCR experiments corroborated the binding of OCT1 to the GLS1 promoter in LX-2 and 293T cells, and knockdown of LOX-1 significantly dampened GLS1 expression (Figure 6D). To further delineate the regulatory domain of OCT1, we cloned the full-length region and four truncations of the GLS1 promoter regions into the pG4.17 basic vector for luciferase reporter assay. We found that LOX-1 knockdown inhibited the transcription of GLS1 via OCT1 (Figure 6E), accordingly, overexpression of LOX-1 induced the activation of the full GLS1 promoter (Fig. S7d). Furthermore, it was observed that LOX-1 knockdown differentially inhibited truncated plasmid luciferase activity, and a binding motif located between −2000 and −1500 was of greatest relevance to OCT1 transcriptional activation of GLS1 (Figure 6F,G). To further substantiate the involvement of LOX-1/GLS1/OTC1 axis in HSC activation, we transfected LX-2 cells with Pou2f1 siRNA. Pou2f1 knockdown decreased expression *Lox-1*, *Gls1* and *Acta2*, *Col1a1* mRNA expression (Fig. S7e). Moreover, simultaneous Pou2f1 silencing attenuated the increased mRNA levels of *Lox-1*, *Gls1* and *Acta2*, *Col1a1* induced by LOX-1overexpression (Fig. S7f). Overall, our findings highlighted the activation of the LOX-1/OCT1/GLS1 axis in HSCs activation and liver fibrogenesis.

3.6. LOX-1 rewired urea cycle/ammonia metabolism to drive liver fibrosis in rats

GLS1, the first enzyme in the glutaminolysis pathway, converts glutamine to glutamate and ammonia [33]. As a by-product of glutamine metabolism, ammonia is considered a toxic substance that must be exported from cells and eliminated through urea cycle activity in the

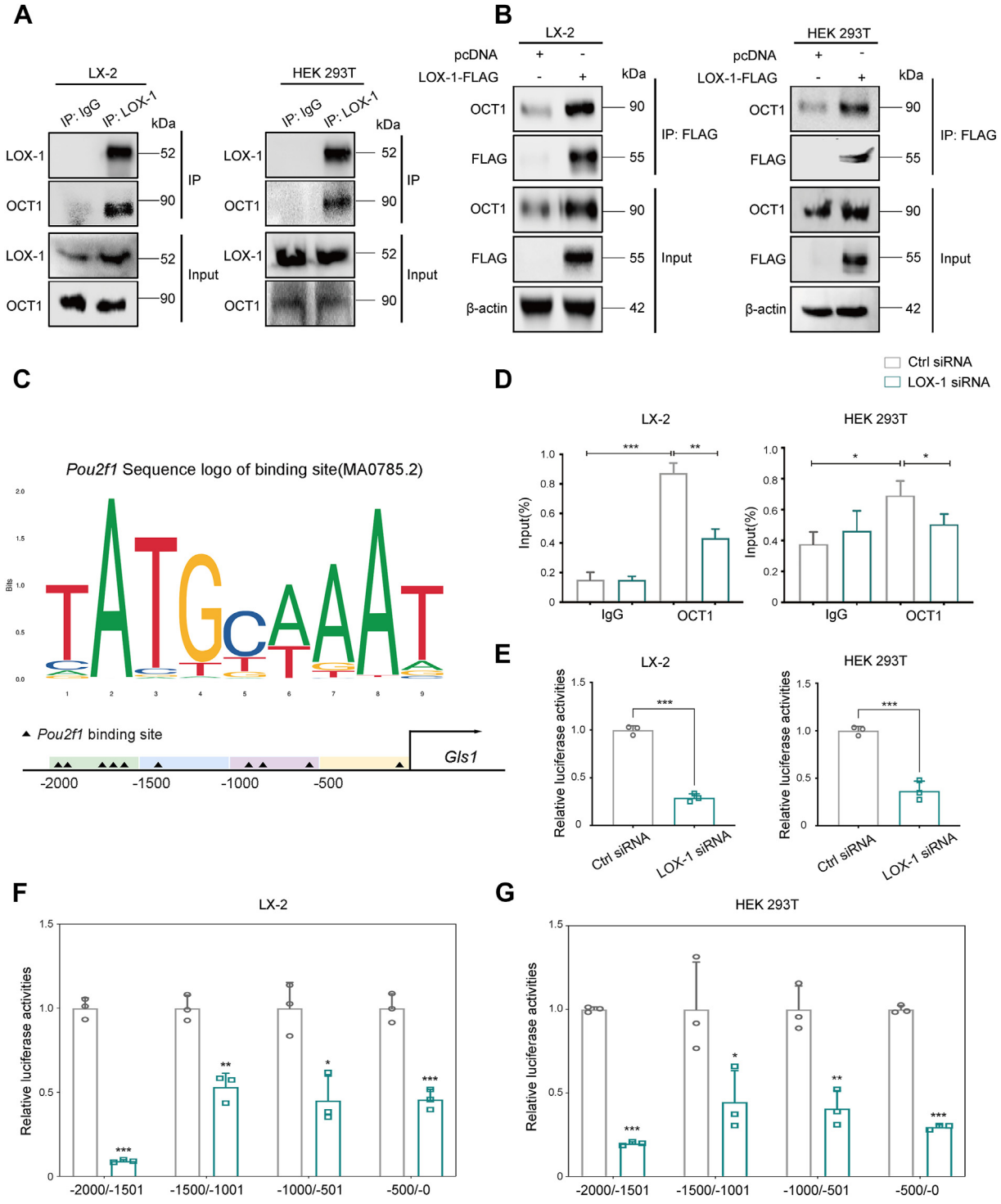

Figure 6: LOX-1 promoted liver fibrosis via OCT1/GLS1 axis. A, Co-immunoprecipitation assays of interaction between LOX-1 and OCT-1 in LX-2 cells (left) and HEK293T cells (right) without treatment. **B**, Co-immunoprecipitation assays of interaction between LOX-1 and OCT-1 in LX-2 cells (left) and HEK293T cells (right) transfected with indicated plasmids. **C**, GLS1 binding motif (JASPAR, https://jaspar.elixir.no/; MA0785.2). **D**, CUT&RUN-qPCR analysis of GLS1 enrichment on *Oct1* in LX-2 cells (left) and HEK293T cells (right) transfected with control siRNA or LOX-1 siRNA. **E**, GLS1 full length promoter-luciferase constructs were transfected into LX-2 cells (left) or HEK29T cells (right) followed by transfection with control siRNA or LOX-1 siRNA. Luciferase activities were examined. **F-G**, GLS1 promoter-luciferase constructs of different lengths were transfected into LX-2 cells (left) or HEK29T cells (right) followed by transfection with control siRNA or LOX-1 siRNA. Luciferase activities were examined. Data are presented as mean ± s.d. *P* values were calculated using one-way ANOVA with Student-Newman-Keuls post hoc analysis (**D**) or a two-tailed Student's *t*-test (**E, F** and **G**); $^{*}P < 0.05$; $^{**}P < 0.01$; $^{***}P < 0.001$.

liver [37]. The urea cycle enzymes, such as ornithine transcarbamoylase (OTC), carbamoylphosphate synthetase-1 (CPS1), argininosuccinate synthetase (ASS1), arginase 1 (ARG1), argininosuccinate lyase (ASL), are responsible for the disposing of 85%—95% of nitrogen waste as urea in the urine [38]. It has been documented that hyperammonemia induces HSCs activation, and reducing ammonia concentration alleviates this activation [27,39]. RNA-seq analysis has provided evidence that genetic LOX-1 deficiency altered the mRNA expression of urea cycle enzymes (OTC, CPS1, ASS1) in fibrotic livers, leading to the question whether LOX-1 exacerbates ammonia disturbance by rewiring the urea cycle (Figure 5B). qPCR analyses confirmed a decrease of OTC, CPS1, ASS1 and ARG1 expression in MCD-induced fibrotic livers, which was abrogated by LOX-1 ablation (Figure 7A). Similarly, OTC, CPS1, ASS1, ARG1 and ASL mRNA expression were downregulated in the CCl_4 model, while significant enhancement of OTC, CPS1 and ASS1 expression was observed in *Lox-1*$^{-/-}$ rats (Fig. S8a). In addition, MCD and CCl_4 led to increased ammonia levels in the liver and plasma of rats, while LOX-1 deficiency reduced ammonia accumulation (Figure 7B,C, Fig. S8b). In line with the in *vivo* results, the deletion of LOX-1 also resulted in a decrease in ammonia levels in activated HSCs (Fig. S8c). Glutamine serves not only as a detoxification product, but also as a means of storing and transportation ammonia [33]. A reduction in ammonia levels was observed in GLS1 knockdown LX-2 cells, but not in GLS2 knockdown LX-2 cells (Fig. S8d). Additionally, BPTES also prevented the accumulation of ammonia caused by LOX-1 overexpression (Fig. S8e). Moreover, we found that inhibiting GLS1 by using BPTES had a significant impact on the expression of urea cycle enzymes (OTC, CPS1) induced by LOX-1 overexpression in LX-2 cells (Fig. S8f). To further explicit the effect of LOX-1 genetic deficiency on glutamine-ammonia metabolism, targeted metabolomics was applied in quantitative analysis of related metabolites. In MCD-induced fibrotic livers, we observed an accumulation of glutamine, citrulline, argininossuccinate and arginine along with a decrease in glutamate levels in *Lox-1*$^{-/-}$ rats, suggesting an increased flux of metabolic recycling of ammonia through glutaminase and urea cycle enzymes (Figure 7D). Besides, MCD feeding and CCl_4 elicited decreased urea levels in the liver tissues, which was elevated by LOX-1 deletion (Figure 7E, Fig. S8g). Since urea cycle enzymes renderes hepatocytes with the ability to achieve the detoxification of ammonia in the form of urea [40], LX-2 cells were treated with NH_4Cl stimulation to simulate a hyperammonia environment in the liver caused by disrupted urea cycle. We found that addition of ammonia exacerbated HSCs activation and disrupted ureagenesis through related metabolic enzymes, but these effects were mitigated in the knockdown of LOX-1 (Figure 7F—G).

Collectively, these findings suggest that LOX-1 contributes to the dysregulation of ammonia homeostasis observed during liver fibrosis. Previous studies have demonstrated that GLS fuels the TCA cycle through glutamine-derived α-ketoglutarate (α-KG), thereby supporting cellular bioenergetics and biosynthetic requirements essential for HSC activation and proliferation [41,42]. To investigate the role of LOX-1 in regulating the glutamine-TCA metabolic network, we supplemented LX-2 cells with DM α-KG (an exogenous form of α-KG) following LOX-1 knockdown or GLS1 inhibition. Our results suggested that supplementation with LX-2 cells with DM α-KG partially rescued the inhibitory effects on HSC activation caused by either LOX-1 knockdow nor GLS1 inhibition alone (Figs. S9a—b). However, simultaneous LOX-1 knockdown and inhibition of GLS1 significantly dimished the rescuing effect of α-KG supplementation (Fig. S9c). These data suggested that LOX-1 potentially enhanced glutaminolysis to sustain TCA cycle flux, and to facilitate HSC activation.

In summary, our results demonstrate that LOX-1 reprograms glutamine metabolism and disrupted urea cycle, leading to elevated ammonia levels, which collectively promote HSC activation and liver fibrosis progression.

4. DISCUSSION

Regardless of aetiology, ECM-producing myofibroblasts are the chief effector cell type contributing to liver fibrosis [1,7]. The goal of this study was to investigate the contribution of LOX-1 to HSCs activation in the progression of liver fibrosis, which has not been previously described. Here, we uncovered a metabolic network through which LOX-1 dysregulated ammonia homeostasis via glutaminolysis and urea cycle during HSCs activation and liver fibrogenesis.

Firstly, we observed a positive correlation between the progression of liver fibrosis and the increase in hepatic LOX-1 expression in both rodents and human patients. Following liver injury, quiescent HSCs undergo activation and transition into α-SMA-positive myofibroblasts, which are the primary source of ECM in fibrotic livers [1,3]. Furthermore, we examined that LOX-1 was predominantly expressed in HSCs, suggesting that LOX-1 may enhance hepatic fibrogenesis via HSCs-myofibroblast transition. Our data exhibited that rats with global genetic LOX-1 deletion were refractory to hepatic fibrosis. Growing evidence portrays a positive association between hepatic free cholesterol levels and the severity of liver histopathology during the transition from MAFL to MASH [43,44]. LOX-1, one of the scavenger receptors for oxLDL, plays a crucial role in the uptake of oxLDL by cells [17,45]. As previously reported, cholesterol accumulation and subsequent foam cell formation in macrophages occures via the scavenger receptor LOX-1, which is up-regulated by oxLDL [18,46,47]. In this setting, we proved that LOX-1 knockout reduced lipid deposition in the fibrotic livers induced by MCD, suggesting that LOX-1 caused hepatic cholesterol accumulation through disruption of cholesterol homeostasis in the pathophysiology of liver fibrogenesis. Subsequently, by means of genetically perturbing LOX-1 in primary HSCs and LX-2 cells, we further validated LOX-1 as a novel target to reverse HSCs-myofibroblast transition. The involvement of LOX-1 in HSCs activation is possibly exacerbated by the high-cholesterol environment, derived from endocytosis of oxLDL by LOX-1. Free cholesterol accumulation in HSCs is increased and further sensitized HSCs to TGF-β1-induced activation in a vicious cycle, leading to exaggerated liver fibrosis [14].

Accumulating evidence supports the crucial role of glutamine metabolism in the pathogenesis of HSCs activation and liver fibrosis [32,48,49]. Attention is drawn to the fact that a metabolic switch from the low-activity GLS2 isoform to the high-activity GLS1 isoform has been observed in end stages of chronic liver disease [34,41,50]. In the present study, transcriptome profiling showed that LOX-1 knockout decreased GLS1 expression and increased GLS2 expression in CCl_4-induced fibrotic livers. As supporting evidence, further results indicated that LOX-1 deficiency suppressed HSCs activation and ameliorated liver fibrosis by reversing the metabolic switch of GLS2 to GLS1. The altered glutaminases in fibrotic livers are likely a direct consequence of metabolic disorder [50], whereas compensatory metabolic networks are activated in the absence of LOX-1 when glutamine metabolism is perturbed. The rationale for how LOX-1 deficiency stimulates this compensatory mechanism remains to be explored intensively.

Our further bioinformatics analysis of transcriptomics implicated GLS1 as a novel target of LOX-1. Dysfunctional synthesis and secretion of VLDL are hallmarks of MASH [51]. Research evidence is available to

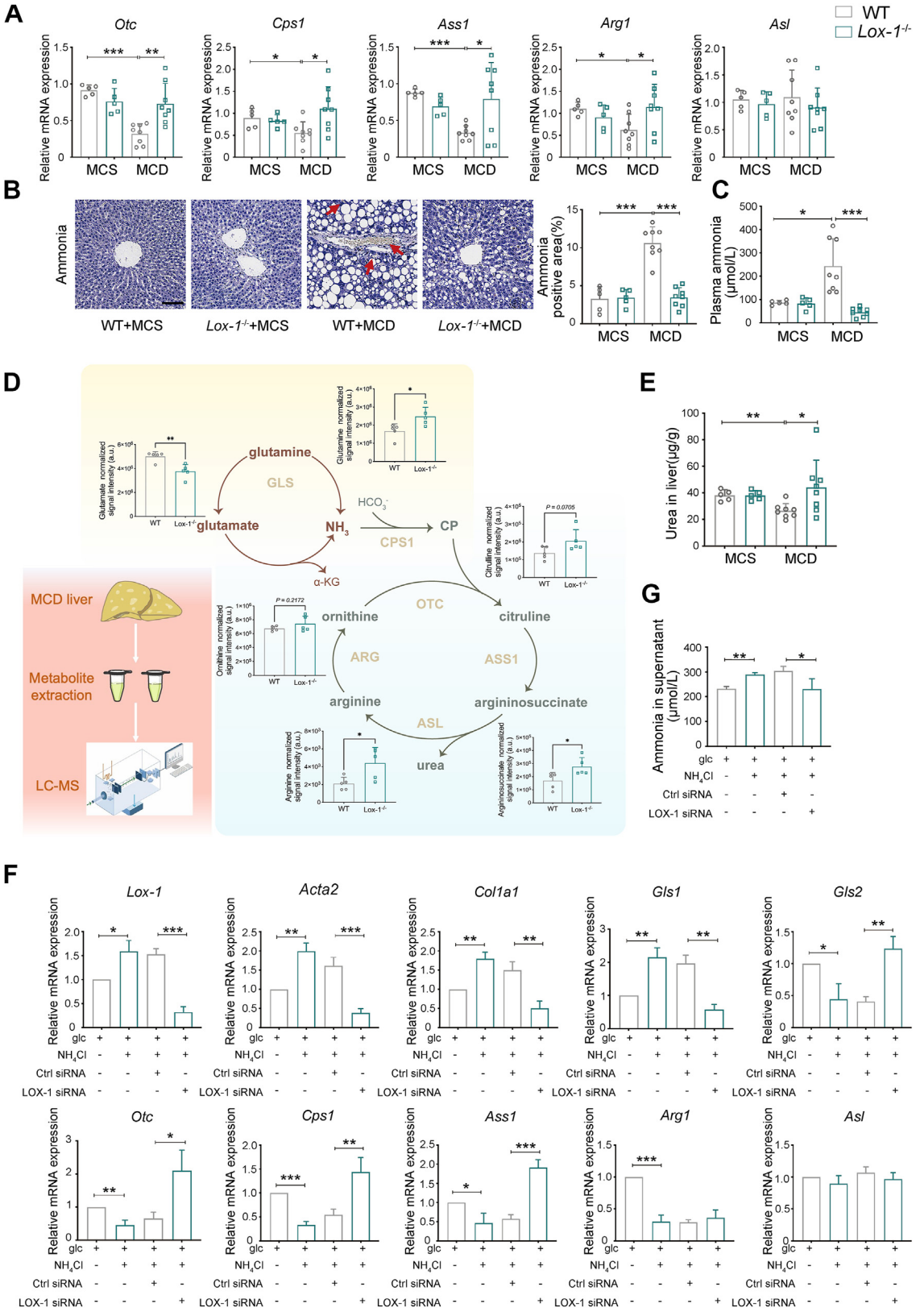

Figure 7: LOX-1 dysregulated nitrogen homeostasis by rewiring urea cycle. A-E, Liver tissues and plasma were harvested from MCD-induced WT and *Lox-1*$^{-/-}$ rats. **A**, Hepatic gene expression of urea cycle enzymes. **B**, Nessler's staining indicating ammonia levels in liver sections. Scale bars, 50 μm. **C**, Ammonia levels in plasma. **D**, Abundance of metabolites. **E**, Urea levels in liver sections. **F-G**, LX-2 cells were transfected with control or LOX-1 siRNA and stimulated with NH_4Cl (4 mM) for 24 h in the presence of glucose (glc). **F**, mRNA levels of fibrogenic genes, glutaminase, urea cycle enzymes. **G**, Ammonia levels in the supernatant. Data are presented as mean ± s.d. *P* values were calculated using one-way ANOVA with Student-Newman-Keuls post hoc analysis (**A-C, E-G**) or a two-tailed Student's *t*-test (**D**); $^{*}P < 0.05$; $^{**}P < 0.01$; $^{***}P < 0.001$.

show that targeting hepatic GLS1 ameliorates MASH by restoring VLDL-TG assembly, suggesting that GLS1 mediates cholesterol efflux, facilitating the progression of MASLD [32]. Our data provided direct evidence supporting the role of LOX-1 in modulating HSCs activation through targeting GLS1, indicating that mutual crosstalk of cholesterol and glutamine metabolism might form a feedback loop engaged in the pathophysiology of liver fibrogenesis. This is consistent with previous findings detailing the involvement of aberrant GLS1-mediated glutaminolysis in HSCs-myofibroblast transition [41]. Our study provided insight into the potential mechanism of LOX-1 in regulating GLS1. Previous researches has provided proof that oxLDL treatment activates the LOX-1/OCT1 signaling pathway in atherosclerosis-related cardiovascular diseases, leading to upregulation of OCT1 levels through oxLDL/LOX-1 binding [30,35,36,52]. Recent work has also demonstrated that OCT1-LOX-1 axis plays a critical role in foam cell formation and cholesterol metabolism [30]. In this regard, our study showed the enhanced interaction of LOX-1 and OCT1 in activated HSCs and fibrotic liver. On the basis of the predicted data from the JASPAR database, we further visualized the transcriptional regulation of the GLS1 promotor by OCT1, which was disrupted in the absence of LOX-1. It's worth noting that this regulatory effect was more evident in the activated HSCs, implying that the LOX-1/OCT1/GLS1 axis held promise as a viable therapeutic approach of liver fibrosis.

Cellular metabolism fuels the bioenergetic and biosynthetic needs of HSCs and paves the way for their activation [10]. In glutamine catabolism, cells are required to properly dispose of the accompanying "by-products" - ammonia, which has been proved to affect HSCs behavior leading to their activation as well as functional and morphological disturbances [39]. The urea cycle is the predominant scavenging metabolic pathway for ammonia [38]. In a rodent model of MASLD induced by a high-fat high-cholesterol diet, a progressive stepwise reduction in the expression and activity of urea cycle enzymes has been observed, resulting in hyperammonemia, evidence of HSCs activation, and progressive fibrosis [27]. Our study verified that rats with steatosis-induced hepatic fibrosis exhibited elevated ammonia levels in both plasma and liver. The cell experiments also demonstrated that a hyperammonia environment triggered HSCs activation while causing diminished expression of urea cycle enzymes, resulting in changes in pertinent metabolites. Since metabolites are involved in different metabolic pathways and have diverse metabolic fates, coordinated metabolism among them is essential for maintaining metabolic homeostasis within cells. Once the changed microenvironment disturbs the balance, a new coordinated metabolism needs to be reestablished. Here, we uncovered that LOX-1 deficiency restored nitrogen homeostasis *in vivo* by inhibiting glutaminolysis and promoting the urea cycle for ammonia clearance, leading to the suppression of HSCs activation and liver fibrogenesis, which is in consonance with prior discoveries [27,53]. Moreover, a recent study has demonstrated that glutamine/ammonia activates lipogenesis in various cancers [54]. Consistently, rerouting amino acid catabolism improves hepatic steatosis, especially glutamine-derived carbons readily fuel fatty acid synthesis in MASLD [55], which promotes the possibility that ammonia and cholesterol metabolism have a mutual influence on each other. In conjunction with our findings, it seems reasonable to think that LOX-1 may be a key mediator that connects ammonia and cholesterol metabolism flows in liver fibrosis.

In addition to providing nitrogen, glutamine serves as an important carbon source supporting cellular bioenergetics and biosynthesis in various myofibrolasts populations [41,56,57]. It has been confirmed that α-KG supplementation enhances GLS1 inhibition and effectively reverses the reduction of GLS1 expression induced by emodin in activated HSCs [41]. Consistently, our results showed that α-KG supplementation reversed the inhibitory effects of either LOX-1 deficiency or GLS1 inhibition alone on HSC activation. However, under conditions of simultaneous LOX-1 knockdown and GLS1 inhibition, HSCs may be subjected to more complex alterations in metabolic and signaling regulatory network. Consequently the rescue effect of α-KG supplementation was dimished in LX-2 cells with combined LOX-1 knockdown and GLS1 inhibition. This suggests that concurrent modulation of LOX-1 and GLS1 may cause profound shifts in metabolic states and signaling cascades in HSCs, making the reactivation of these cells more challenging through α-KG supplementation alone. Recent research revealed that perturbations in the hierarchical urea-TCA cycle controlled via arginase might link urea cycle compromise to fibroinflammatory liver disease [58,59]. Incorporating our findings on LOX-1 regulation of urea cycle, it suggested that LOX-1 might rewire glutamine metabolism to perturb hierarchical urea-TCA cycle regulation driving the progression of liver fibrosis. Further in-depth investigations are required to elucidate the detailed mechanisms underlying this metabolic crosstalk and its implications in fibrosis progression.

However, this study had several limitations. Our present sudy concentrated on the involvement of LOX-1 in activated HSCs, whereas the specific source of LOX-1 within the intricate context of liver fibrosis remains to be definitively established. To confirm the effect of targeting LOX-1 in HSCs on liver fibrosis, constructing HSCs-specific LOX-1 knockout mice would be necessary. In addition, considering that the urea cycle occurs in hepatocytes [38], whether targeting LOX-1 inhibits HSCs activation stimulated by waste ammonia accumulation in hepatocytes requires to be validated. In this setting, we also interestingly found that LOX-1 co-localized with ALBUMIN in CCl4-induced mice fibrotic livers (Fig. S1d). We therefore propose to further investigated the mechanism of LOX-1 regulation of ammonia metabolism in hepatocyte-specific LOX-1 knockout mice.

In conclusion, the expression of LOX-1 was found to be significantly elevated in fibrotic/cirrhotic liver tissues with various etiologies of liver disease. The upregulation of LOX-1 played a pivotal role in the development and progression of liver fibrosis through the activation of the LOX-1/OCT1/GLS1 axis. Further clarification of the LOX-1-influenced glutamine-ammonia metabolic cycle could potentially reveal additional strategies to impede the deterioration of liver fibrosis. Our results emphasize the importance of targeting LOX-1 for the prevention and treatment of fibrosis progression, and shed light on the potential clinical application.

ACKNOWLEDGMENTS

We cordially wish to acknowledge Xiangya Hospital Central South University for providing patient liver tissues. This work was supported by National Natural Science Foundation of China (No. 82204489, 82241025, 82173817), Natural Science Foundation of Hunan Province (No. 211142095031), Foundation of Hunan Educational Committee (No. 23B0018), Young Elite Scientists Sponsorship Program by CAST (No. 2023QNRC001) to Xiaoyun Zhu.

CRediT AUTHORSHIP CONTRIBUTION STATEMENT

Ruihua Huang: Writing — review & editing, Writing — original draft, Visualization, Data curation, Conceptualization. **Hanyu Cui:** Validation, Formal analysis, Data curation. **Mohammed Abdulaziz Yahya Ali Alshami:** Formal analysis, Data curation. **Chuankui Fu:** Validation, Data curation. **Wei Jiang:** Validation, Data curation. **Mingyuan Cai:**

Validation, Formal analysis. **Shuhan Zhou:** Validation, Data curation. **Xiaoyun Zhu:** Writing — review & editing, Supervision, Resources, Project administration, Funding acquisition. **Changping Hu:** Writing — review & editing, Supervision, Project administration, Funding acquisition, Conceptualization.

DECLARATION OF COMPETING INTEREST

The authors declare that they have no known competing financial interests or personal relationships that could have appeared to influence the work reported in this paper.

DATA AVAILABILITY

Data will be made available on request.

APPENDIX A. SUPPLEMENTARY DATA

Supplementary data to this article can be found online at https://doi.org/10.1016/j.molmet.2025.102132.

REFERENCES

[1] Kisseleva T, Brenner D. Molecular and cellular mechanisms of liver fibrosis and its regression. Nat Rev Gastroenterol Hepatol 2021;18(3):151—66. https://doi.org/10.1038/s41575-020-00372-7.

[2] Pellicoro A, Ramachandran P, Iredale JP, Fallowfield JA. Liver fibrosis and repair: immune regulation of wound healing in a solid organ. Nat Rev Immunol 2014;14(3):181—94. https://doi.org/10.1038/nri3623.

[3] Yang X, Li Q, Liu W, Zong C, Wei L, Shi Y, et al. Mesenchymal stromal cells in hepatic fibrosis/cirrhosis: from pathogenesis to treatment. Cell Mol Immunol 2023;20(6):583—99. https://doi.org/10.1038/s41423-023-00983-5.

[4] Hammerich L, Tacke F. Hepatic inflammatory responses in liver fibrosis. Nat Rev Gastroenterol Hepatol 2023;20(10):633—46. https://doi.org/10.1038/s41575-023-00807-x.

[5] Taru V, Szabo G, Mehal W, Reiberger T. Inflammasomes in chronic liver disease: hepatic injury, fibrosis progression and systemic inflammation. J Hepatol 2024;81(5):895—910. https://doi.org/10.1016/j.jhep.2024.06.016.

[6] Friedman SL. Mechanisms of hepatic fibrogenesis. Gastroenterology 2008;134(6):1655—69. https://doi.org/10.1053/j.gastro.2008.03.003.

[7] Hernandez-Gea V, Friedman SL. Pathogenesis of liver fibrosis. Annu Rev Pathol 2011;6:425—56. https://doi.org/10.1146/annurev-pathol-011110-130246.

[8] Huang DQ, Mathurin P, Cortez-Pinto H, Loomba R. Global epidemiology of alcohol-associated cirrhosis and hcc: trends, projections and risk factors. Nat Rev Gastroenterol Hepatol 2023;20(1):37—49. https://doi.org/10.1038/s41575-022-00688-6.

[9] Keam SJ. Resmetirom: first approval. Drugs 2024;84(6):729—35. https://doi.org/10.1007/s40265-024-02045-0.

[10] Trivedi P, Wang S, Friedman SL. The power of plasticity-metabolic regulation of hepatic stellate cells. Cell Metab 2021;33(2):242—57. https://doi.org/10.1016/j.cmet.2020.10.026.

[11] Tsuchida T, Friedman SL. Mechanisms of hepatic stellate cell activation. Nat Rev Gastroenterol Hepatol 2017;14(7):397—411. https://doi.org/10.1038/nrgastro.2017.38.

[12] Higashi T, Friedman SL, Hoshida Y. Hepatic stellate cells as key target in liver fibrosis. Adv Drug Deliv Rev 2017;121:27—42. https://doi.org/10.1016/j.addr.2017.05.007.

[13] Li H, Yu XH, Ou X, Ouyang XP, Tang CK. Hepatic cholesterol transport and its role in non-alcoholic fatty liver disease and atherosclerosis. Prog Lipid Res 2021;83:101109. https://doi.org/10.1016/j.plipres.2021.101109.

[14] Tomita K, Teratani T, Suzuki T, Shimizu M, Sato H, Narimatsu K, et al. Free cholesterol accumulation in hepatic stellate cells: mechanism of liver fibrosis aggravation in nonalcoholic steatohepatitis in mice. Hepatology 2014;59(1):154—69. https://doi.org/10.1002/hep.26604.

[15] Duan Y, Gong K, Xu S, Zhang F, Meng X, Han J. Regulation of cholesterol homeostasis in health and diseases: from mechanisms to targeted therapeutics. Signal Transduct Targeted Ther 2022;7(1):265. https://doi.org/10.1038/s41392-022-01125-5.

[16] Mehta JL, Sanada N, Hu CP, Chen J, Dandapat A, Sugawara F, et al. Deletion of lox-1 reduces atherogenesis in ldlr knockout mice fed high cholesterol diet. Circ Res 2007;100(11):1634—42.

[17] Moore KJ, Freeman MW. Scavenger receptors in atherosclerosis: beyond lipid uptake. Arterioscler Thromb Vasc Biol 2006;26(8):1702—11. https://doi.org/10.1161/01.Atv.0000229218.97976.43.

[18] Chistiakov DA, Melnichenko AA, Myasoedova VA, Grechko AV, Orekhov AN. Mechanisms of foam cell formation in atherosclerosis. J Mol Med (Berl) 2017;95(11):1153—65. https://doi.org/10.1007/s00109-017-1575-8.

[19] Zhang J, Yang P, Wang H, Huang Q, Chen T, Li N, et al. N-3 pufas inhibited hepatic er stress induced by feeding of a high-saturated fat diet accompanied by the expression lox-1. J Nutr Biochem 2021;88:108481. https://doi.org/10.1016/j.jnutbio.2020.108481.

[20] Ho C-M, Ho S-L, Jeng Y-M, Lai Y-S, Chen Y-H, Lu S-C, et al. Accumulation of free cholesterol and oxidized low-density lipoprotein is associated with portal inflammation and fibrosis in nonalcoholic fatty liver disease. J Inflamm 2019;16:7. https://doi.org/10.1186/s12950-019-0211-5.

[21] Musso G, Cassader M, De Michieli F, Saba F, Bo S, Gambino R, et al. Effect of lectin-like oxidized ldl receptor-1 polymorphism on liver disease, glucose homeostasis, and postprandial lipoprotein metabolism in nonalcoholic steatohepatitis. Am J Clin Nutr 2011;94(4):1033—42. https://doi.org/10.3945/ajcn.111.015610.

[22] Kang Q, Chen A. Curcumin eliminates oxidized ldl roles in activating hepatic stellate cells by suppressing gene expression of lectin-like oxidized ldl receptor-1. Lab Invest 2009;89(11):1275—90. https://doi.org/10.1038/labinvest.2009.93.

[23] Li X, Tang X, Liu B, Zhang J, Zhang Y, Lv H, et al. Lox-1 deletion attenuates myocardial fibrosis in the aged mice, particularly those with hypertension. Front Cardiovasc Med 2021;8:736215. https://doi.org/10.3389/fcvm.2021.736215.

[24] Zou XZ, Gong ZC, Liu T, He F, Zhu TT, Li D, et al. Involvement of epithelial-mesenchymal transition afforded by activation of lox-1/tgf-β1/klf6 signaling pathway in diabetic pulmonary fibrosis. Pulm Pharmacol Ther 2017;44:70—7. https://doi.org/10.1016/j.pupt.2017.03.012.

[25] Zhang Y, Zhang R, Lu L, Zhou N, Lv X, Wang X, et al. Knockdown of lectin-like oxidized low-density lipoprotein-1 ameliorates alcoholic cardiomyopathy via inactivating the p38 mitogen-activated protein kinase pathway. Bioengineered 2022;13(4):8926—36. https://doi.org/10.1080/21655979.2022.2056814.

[26] Ge X, Zhang W, Zhu T, Huang N, Yao M, Liu H, et al. Hypoxia-activated platelets stimulate proliferation and migration of pulmonary arterial smooth muscle cells by phosphatidylserine/lox-1 signaling-impelled intercellular communication. Cell Signal 2021;87:110149. https://doi.org/10.1016/j.cellsig.2021.110149.

[27] De Chiara F, Thomsen KL, Habtesion A, Jones H, Davies N, Gracia-Sancho J, et al. Ammonia scavenging prevents progression of fibrosis in experimental nonalcoholic fatty liver disease. Hepatology 2020;71(3):874—92. https://doi.org/10.1002/hep.30890.

[28] Zhu X, Zhang Y, Zhao Y, Xiang D, Zou J, Andrisani O, et al. Lix1-like protein drives hepatic stellate cell activation to promote liver fibrosis by regulation of chemokine mrna stability. Signal Transduct Targeted Ther 2021;6(1):319. https://doi.org/10.1038/s41392-021-00665-6.

[29] Mederacke I, Dapito DH, Affo S, Uchinami H, Schwabe RF. High-yield and high-purity isolation of hepatic stellate cells from normal and fibrotic mouse livers. Nat Protoc 2015;10(2):305—15. https://doi.org/10.1038/nprot.2015.017.

[30] Fan J, Liu L, Liu Q, Cui Y, Yao B, Zhang M, et al. Ckip-1 limits foam cell formation and inhibits atherosclerosis by promoting degradation of oct-1 by regγ. Nat Commun 2019;10(1):425. https://doi.org/10.1038/s41467-018-07895-3.

[31] Du K, Chitneni SK, Suzuki A, Wang Y, Henao R, Hyun J, et al. Increased glutaminolysis marks active scarring in nonalcoholic steatohepatitis progression. Cell Mol Gastroenterol Hepatol 2020;10(1):1—21. https://doi.org/10.1016/j.jcmgh.2019.12.006.

[32] Simon J, Nuñez-García M, Fernández-Tussy P, Barbier-Torres L, Fernandez-Ramos D, Gomez-Santos B, et al. Targeting hepatic glutaminase 1 ameliorates non-alcoholic steatohepatitis by restoring very-low-density lipoprotein triglyceride assembly. Cell Metab 2020;31(3):605—22. https://doi.org/10.1016/j.cmet.2020.01.013.

[33] Yoo HC, Yu YC, Sung Y, Han JM. Glutamine reliance in cell metabolism. Exp Mol Med 2020;52(9):1496—516. https://doi.org/10.1038/s12276-020-00504-8.

[34] Zhang L, Su K, Liu Q, Li B, Wang Y, Cheng C, et al. Kidney-type glutaminase is a biomarker for the diagnosis and prognosis of hepatocellular carcinoma: a prospective study. BMC Cancer 2023;23(1):1081. https://doi.org/10.1186/s12885-023-11601-y.

[35] Chen J, Liu Y, Liu H, Hermonat PL, Mehta JL. Lectin-like oxidized low-density lipoprotein receptor-1 (lox-1) transcriptional regulation by oct-1 in human endothelial cells: implications for atherosclerosis. Biochem J 2006;393(Pt 1):255—65. https://doi.org/10.1042/bj20050845.

[36] Akhmedov A, Camici GG, Reiner MF, Bonetti NR, Costantino S, Holy EW, et al. Endothelial lox-1 activation differentially regulates arterial thrombus formation depending on oxldl levels: role of the oct-1/sirt1 and erk1/2 pathways. Cardiovasc Res 2017;113(5):498—507. https://doi.org/10.1093/cvr/cvx015.

[37] Lercher A, Bhattacharya A, Popa AM, Caldera M, Schlapansky MF, Baazim H, et al. Type i interferon signaling disrupts the hepatic urea cycle and alters systemic metabolism to suppress t cell function. Immunity 2019;51(6). https://doi.org/10.1016/j.immuni.2019.10.014.

[38] Keshet R, Szlosarek P, Carracedo A, Erez A. Rewiring urea cycle metabolism in cancer to support anabolism. Nat Rev Cancer 2018;18(10):634—45. https://doi.org/10.1038/s41568-018-0054-z.

[39] Jalan R, De Chiara F, Balasubramaniyan V, Andreola F, Khetan V, Malago M, et al. Ammonia produces pathological changes in human hepatic stellate cells and is a target for therapy of portal hypertension. J Hepatol 2016;64(4):823—33. https://doi.org/10.1016/j.jhep.2015.11.019.

[40] Hajaj E, Sciacovelli M, Frezza C, Erez A. The context-specific roles of urea cycle enzymes in tumorigenesis. Mol Cell 2021;81(18):3749—59. https://doi.org/10.1016/j.molcel.2021.08.005.

[41] Du K, Hyun J, Premont RT, Choi SS, Michelotti GA, Swiderska-Syn M, et al. Hedgehog-yap signaling pathway regulates glutaminolysis to control activation of hepatic stellate cells. Gastroenterology 2018;154(5):1465—1479.e1413. https://doi.org/10.1053/j.gastro.2017.12.022.

[42] Yin XC, Peng J, Gu LH, Liu Y, Li X, Wu J, et al. Targeting glutamine metabolism in hepatic stellate cells alleviates liver fibrosis. Cell Death Dis 2022;13(11). ARTN 95510.1038/s41419-022-05409-0.

[43] Ioannou GN. The role of cholesterol in the pathogenesis of nash. Trends Endocrinol Metabol 2016;27(2):84—95. https://doi.org/10.1016/j.tem.2015.11.008.

[44] Puri P, Baillie RA, Wiest MM, Morshahi F, Choudhury J, Cheung O, et al. A lipidomic analysis of nonalcoholic fatty liver disease. Hepatology 2007;46(4):1081—90. https://doi.org/10.1002/hep.21763.

[45] Pothineni NVK, Karathanasis SK, Ding Z, Arulandu A, Varughese KI, Mehta JL. Lox-1 in atherosclerosis and myocardial ischemia: biology, genetics, and modulation. J Am Coll Cardiol 2017;69(22):2759—68. https://doi.org/10.1016/j.jacc.2017.04.010.

[46] Luchetti F, Crinelli R, Nasoni MG, Benedetti S, Palma F, Fraternale A, et al. Ldl receptors, caveolae and cholesterol in endothelial dysfunction: oxldls accomplices or victims? Br J Pharmacol 2021;178(16):3104—14. https://doi.org/10.1111/bph.15272.

[47] Steinberg D. Atherogenesis in perspective: hypercholesterolemia and inflammation as partners in crime. Nat Med 2002;8(11):1211—7. https://doi.org/10.1038/nm1102-1211.

[48] Wang F, Li Z, Chen L, Yang T, Liang B, Zhang Z, et al. Inhibition of asct2 induces hepatic stellate cell senescence with modified proinflammatory secretome through an il-1α/nf-κb feedback pathway to inhibit liver fibrosis. Acta Pharm Sin B 2022;12(9):3618—38. https://doi.org/10.1016/j.apsb.2022.03.014.

[49] Chen L, Liang B, Xia S, Wang F, Li Z, Shao J, et al. Emodin promotes hepatic stellate cell senescence and alleviates liver fibrosis via a nuclear receptor (nur77)-mediated epigenetic regulation of glutaminase 1. Br J Pharmacol 2023;180(19):2577—98. https://doi.org/10.1111/bph.16156.

[50] Yuneva MO, Fan TW, Allen TD, Higashi RM, Ferrari DV, Tsukamoto T, et al. The metabolic profile of tumors depends on both the responsible genetic lesion and tissue type. Cell Metab 2012;15(2):157—70. https://doi.org/10.1016/j.cmet.2011.12.015.

[51] Fujita K, Nozaki Y, Wada K, Yoneda M, Fujimoto Y, Fujitake M, et al. Dysfunctional very-low-density lipoprotein synthesis and release is a key factor in nonalcoholic steatohepatitis pathogenesis. Hepatology 2009;50(3):772—80. https://doi.org/10.1002/hep.23094.

[52] Neri Serneri GG, Coppo M, Bandinelli M, Paoletti P, Toscano T, Micalizzi E, et al. Exaggerated myocardial oxldl amount and lox-1 receptor over-expression associated with coronary microvessel inflammation in unstable angina. Atherosclerosis 2013;226(2):476—82. https://doi.org/10.1016/j.atherosclerosis.2012.11.007.

[53] De Chiara F, Heebøll S, Marrone G, Montoliu C, Hamilton-Dutoit S, Ferrandez A, et al. Urea cycle dysregulation in non-alcoholic fatty liver disease. J Hepatol 2018;69(4):905—15. https://doi.org/10.1016/j.jhep.2018.06.023.

[54] Cheng C, Geng F, Li Z, Zhong Y, Wang H, Cheng X, et al. Ammonia stimulates scap/insig dissociation and srebp-1 activation to promote lipogenesis and tumour growth. Nat Metab 2022;4(5):575—88. https://doi.org/10.1038/s42255-022-00568-y.

[55] Liao YL, Chen QS, Liu L, Huang H, Sun J, Bai X, et al. Amino acid is a major carbon source for hepatic lipogenesis. Cell Metab 2024;36(11):2347—448. https://doi.org/10.1016/j.cmet.2024.10.001.

[56] Yang HY, Tsai CY, Chen KH, Yang CW. Glutamine metabolism inhibition alleviates kidney fibrosis through the immunometabolic axis. J Am Soc Nephrol 2024;35(10). https://doi.org/10.1681/ASN.2024ajgaztbr.

[57] Contento G, Wilson J a a M, Selvarajah B, Plate M, Guillotin D, Morales V, et al. Pyruvate metabolism dictates fibroblast sensitivity to gls1 inhibition during fibrogenesis. Jci Insight 2024;9(18):e178453. ARTN e17845310.1172/jci.insight.178453.

[58] Zhang YM, Higgins CB, Tica S, Adams JA, Sun J, Kelly SC, et al. Hierarchical tricarboxylic acid cycle regulation by hepatocyte arginase 2 links the urea cycle to oxidative metabolism. Cell Metab 2024;36(9):2069—85. https://doi.org/10.1016/j.cmet.2024.07.007.

[59] Gallego-Durán R, Hadjihambi A, Ampuero J, Rose CF, Jalan R, Romero-Gomez M. Ammonia-induced stress response in liver disease progression and hepatic encephalopathy. Nat Rev Gastroenterol Hepatol 2024;21(11):774—91. https://doi.org/10.1038/s41575-024-00970-9.

